Mechanical Systems and Signal Processing 147 (2021) 107068

Contents lists available at ScienceDirect

Mechanical Systems and Signal Processing

journal homepage: www.elsevier.com/locate/ymssp

Frequency energy shift method for bearing fault prognosis using microphone sensor

Jaewoong Park [1], Seokgoo Kim [1], Joo-Ho Choi *, Seung Hwan Lee *

School of Aerospace and Mechanical Engineering, Korea Aerospace University, 76 Hanggongdae-gil, Deokyang-gu, Goyang-si, Gyeonggi-do 10540, Republic of Korea

ARTICLE INFO

Article history:
Received 18 October 2019
Received in revised form 9 April 2020
Accepted 11 June 2020
Available online 3 July 2020

Keywords:
Bearing
Run-to-fail (RTF)
Natural fault
Acoustic sensor
Frequency energy shifting method (FESM)
Anomaly detection
Prognosis

ABSTRACT

A novel health index is proposed to detect incipient fault of ball bearing and monitor its progression earlier than the visible fault appearance using the microphone sensor. Frequency energy shift method is employed to extract the health index (HI), based on the findings that the energy is concentrated and shifted in specific frequency bands as the fault progresses. In the early stage, the anomaly of incipient fault is detected by the Chi-square test of HI. The end of life where visible faults appear is defined by the moment when the raw signal and its envelope spectrum at fault frequencies show distinct increase. Natural faults made by run-to-fail (RTF) experiments are used to demonstrate the approach. The performance of HI using the microphone sensor is superior to that of vibration due to the advantage of non-contact sensing. It successfully indicates early fault detection and damage progression before the visible faults show up.

1. Introduction

As the size of industry grows and technology becomes more sophisticated, a small defect of the bearings in the complex systems can cause critical loss and damage, which are occasionally found in the railways, automobiles, power plants, machine tools and many others. Despite many efforts, the accidents caused by the bearing defects in the railway, for example, have been constantly reported over the years [1,2]. Therefore, it is very important to develop a solution to detect incipient fault of bearing by condition monitoring and predict its remaining life during the operation [3–5]. However, it is difficult to acquire natural fault data developing under the real operating environments.

Due to this constraint, more researches have been directed to the diagnosis study by seeding artificial faults to the bearings in the test rig, in which the sensor signals are measured. Among the available sensors, the accelerometer has been most common and cost-effective to analyze the fault characteristics of the bearing during operation [6]. However, it has the drawbacks of interference with other signals and difficulty of attachment within the system. Acoustic non-contact sensors such as microphone are recently drawing attention as an alternative, particularly in the railways application, which detects the pressure wave generated by the bearing [7]. Several studies have been made in this direction. Zhang et al. have conducted to diagnose multiple bearing faults made artificially at the inner, outer ring and roller, using the microphones mounted on the wayside of rail. A time-varying spatial filtering rearrangement (TSFR) method is applied for the fault diagnosis [3]. Zhang et al. have employed microphones for the features extraction from the fault-seeded bearing in the laboratory as well as in the

* Corresponding authors.
E-mail addresses: jhchoi@kau.ac.kr (J.-H. Choi), seunglee@kau.ac.kr (S.H. Lee).
[1] Equally contributed as first authors, Graduate students.

https://doi.org/10.1016/j.ymssp.2020.107068
0888-3270/

field respectively. Improved singular value decomposition (ISVD) and resonance-based signal sparse decomposition (RSSD) are employed to separate the fault signal for the diagnosis [8]. Akcay et al. have used several microphones to detect artificial fault in the bearing of induction motor to find that the pressure of the defective motor increases by 8 dB. Subspace-based system identification method is used to estimate the power spectrum density (PSD) [9]. Mohanty et al. have used an accelerometer and microphone in concert in their bearing experiments. Empirical and variational mode decomposition (EMD and VMD) are used for the fault features extraction, from which they found that the VMD is better than the EMD at variable speed conditions [10]. Glowacz have used a microphone to diagnose the bearing failure of a single-phase induction motor, which are naturally damaged over long-time operation. Using the frequency spectrum difference of the acoustic signal, normal and defective bearings are classified by the k-nearest neighbor (kNN) algorithm with 97% accuracy [11]. Eftekharnejad et al. have investigated the feasibility of contact-type acoustic and vibration sensors for the detection of naturally degraded bearing faults. Spectral kurtosis (SK) and kurtogram are used for the features extraction, in which the contact type acoustic sensors are found more sensitive than the vibration sensors in identifying the incipient bearing faults [12]. In most of the above literature, it is apparent that the artificial faults are used in the diagnosis. However, the artificial faults tend to produce cleaner signal than those from the naturally-born faults, which limits its application in the real field. Furthermore, while the diagnosis focuses on the fault identification after its occurrence, the prognosis involves detecting onset of defect and predicting fault progression over cycles, which is of more significance in the maintenance. In general, prognosis is performed by introducing a proper health index (HI) from the measured signals, using which the current health status is estimated and its future is predicted. There have been a lot of researches in this direction, but they were predominantly developed for the vibration signals. Upon survey of literature, most approaches have been driven by the features from the statistical ones such as rms and kurtosis, the frequency domain features, and the bearing fault frequencies commonly used in the fault diagnosis. Table 1 provides a summary of few selected approaches in view of the feature extraction for HI construction. Further details of these approaches are described in the authors' paper [13]. The main idea is to select features with high correlation with fault progression, and convert them into a single index. Regarding the HI study using the microphone signals, however, no papers are found to date to the authors' knowledge.

In this study, motivated by the above issues, natural faults are developed by the RTF operations from the normal bearings in a test rig, in which a microphone is placed with close distance to the bearing to detect incipient faults and trace its progression over time. Frequency energy shift method (FESM) is proposed to extract a health index (HI) suited for this purpose, which is rooted on the findings that the bearing faults are caused by energy concentration/shift in the specific frequency bands during the fault development over cycles. Using the HI, anomaly is detected at the early stage, which is supposed as the moment the incipient fault develops. Defining the end of life as the time when the visible spall appears, the corresponding threshold is provided by examining the raw acoustic signal as well as its envelope spectra at fault frequencies. Then the HI is monitored over time as a means of assessing current health indicator against the failure threshold.

2. Experiment and measured data

2.1. Experimental setup

Fig. 1 shows the bearing test rig in which the RTF tests are performed. The test rig consists of sensors, test bearings, support bearings, motor, DAQ boards, and data storage. The sensors used in this study are a microphone (PCB Piezotronics 378C01), an accelerometer (KS77C.100 by MMF) and a thermocouple (RTD of NI). The DAQ boards consist of NI Pxle-4464 and NI-9212, in which the former records acoustic and vibration signals at a sample rate of 204.8 k/s, and the latter records the temperature at a sample rate of 100 Hz. The first 1 s of every 10 s is stored due to the size of the data. LabVIEW software is used to control the system.

Fig. 2 shows the configuration of the ball bearing, NSK 7202BW. The specification of the ball bearing is given by Table 2. For the experimental setup, as an initial step, the NSK 7202BW is inserted into the shaft as shown in Fig. 1(b) and retaining rings are added around the support bearings, as shown in Fig. 1(c). Then the sensors are positioned as shown in Fig. 1(b). The microphone is installed at a horizontal distance of 100 mm from the test bearing. The accelerometer is attached to the right of the bearing housing. The thermocouple is located 15 mm upward from the bearing. Then the bearing is tested under the shaft rotation at 1700 rpm. Considering that many bearings are located at the end of the wheels or axles as found in the automotive and railways, the bearing in this study is positioned at the left end of the shaft as shown in Fig. 1(b). Radial load generated by the mechanical fastening of bolts is applied to the test bearing from upward at 75~80% of the dynamic load rating of 7950 N to develop natural growing defects during the operation. Due to the configuration that the load is exerted at the end of the shaft, the shaft tends to move toward the negative $\times$ direction. To prevent this, coupling is fastened more securely between the motor and the shaft, and the retaining rings are added around the support bearings. During the RTF tests, substantial noise is generated over time due to the wear between the support bearings and shaft. Though the noise could adversely affect fault signal detection, instead of fixing the problem, the test rig is operated as it is, assuming that the noise may represent the real situation in the field, and the measured signal is used for the prognosis study. After a number of trials to ensure the faults fully developed over cycles while maintaining safe operations, the test is terminated after less than 20 min when the acoustic pressure, acceleration and temperature exceed the thresholds of 9 Pascal, 18 m/s^2 and 80 °C, simultaneously.

Table 1
Summary of existing approaches for HI construction in the bearing prognostics.

Ref.	Prognostic feature
Siegel et al. [14]	Top 20 are selected from TDFs and FFAs by correlation metric. Then SOM distance is then used
Sutrisnoet al. [15]	Average of 5 highest absolute acceleration values
Camci et al. [16]	12 TDFs of raw, low pass & high passed signals, leading to total of 36 signals
Zhang et al. [17]	Sum of all FFAs in weighted frequency band
Wu et al. [18]	Among TDFs, FFAs and IMFs of EEMD, features are selected via 3 metrics from RTF data. Then dynamic PCA and MD are used to extract a single feature
Loutas et al. [19]	Among 60 s from TDFs, FFAs and WPD, monotonic features are chosen by RTF data. SVR is used without extracting single feature.
An et al. [20]	Information entropy based on amplitude change at specific frequencies
Qiu et al. [21]	WT features are used to get SOM based prognostic feature
Guo et al. [22]	Among 6 related-similarity features from TDFs & 5 frequency spectra, features are selected via 3 metrics from RTF data. Then RNN-HI is constructed
Rai et al. [23]	GMM and JRD using the IMFs of EEMD
Duan et al. [24]	Multi-dimensional cumulative transformations of TDFs, FDFs and WTs are fused into kernel PCA
Jin et al. [25]	Residuals made by AR training of RTF data are used to obtain wavelet features, from which MD is applied to get the feature
Baraldi et al. [26]	IMFs of EMD extracted by AAKR
Yu [27]	12 TDFs and FDFs by combination of GMM and k-means
Liu et al. [28]	Among the 14 AE features constructed using PCA after data mining

TDF: Time-domain feature; FFA: Fault frequency amplitude; SOM: Self-organizing map; IMF: Intrinsic mode function; EEMD: Ensemble empirical mode decomposition; PCA: Principal component analysis; MD: Mahalanobis distance; WPD: Wavelet packet decomposition; SVR: Support vector regression; WT: Wavelet transform; FDF: Frequency-domain feature; RNN-HI: Recurrent neural network-based health indicator; GMM: Gaussian mixture models; JRD: Jensen–Rényi divergence; AR: Autoregressive; AAKR: Auto-associative kernel regression; AE: Acoustic emission.

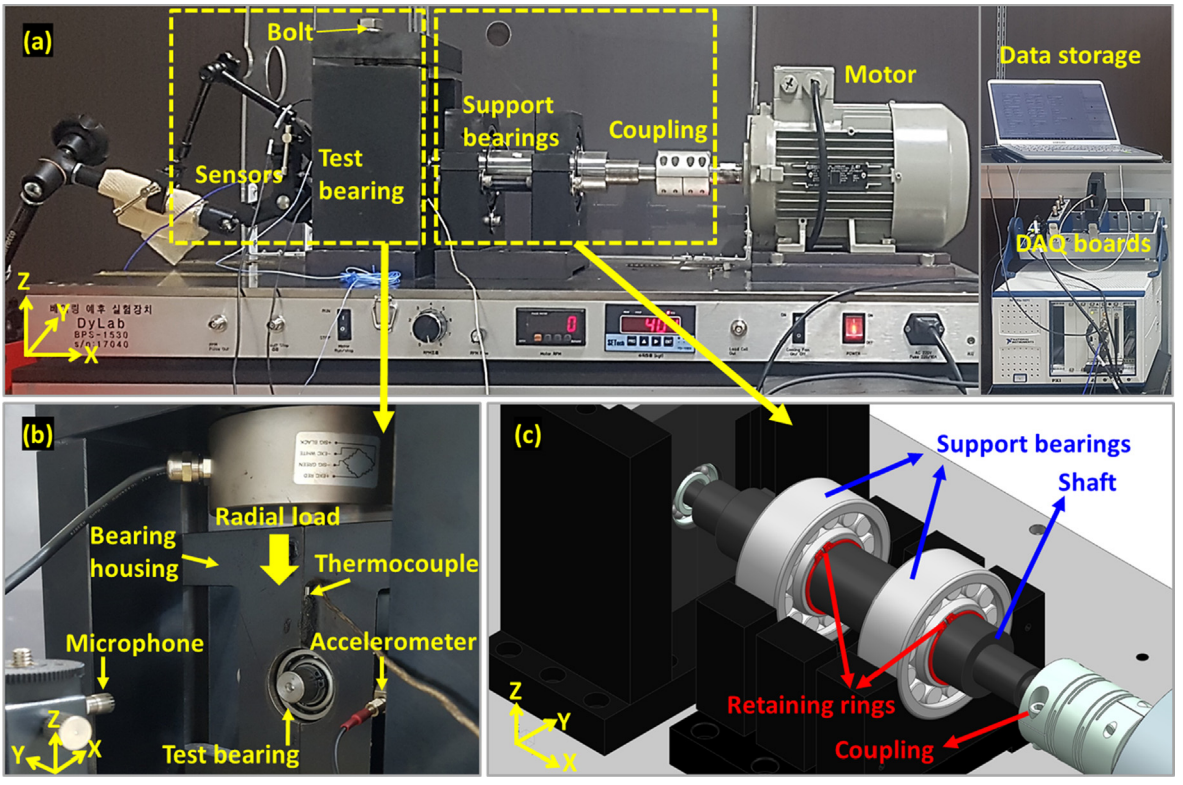

Fig. 1. The bearing test rig: (a) Front view of the bearing test rig, (b) Close up view of test bearing and sensors (c) Close up view of support bearings and couplings

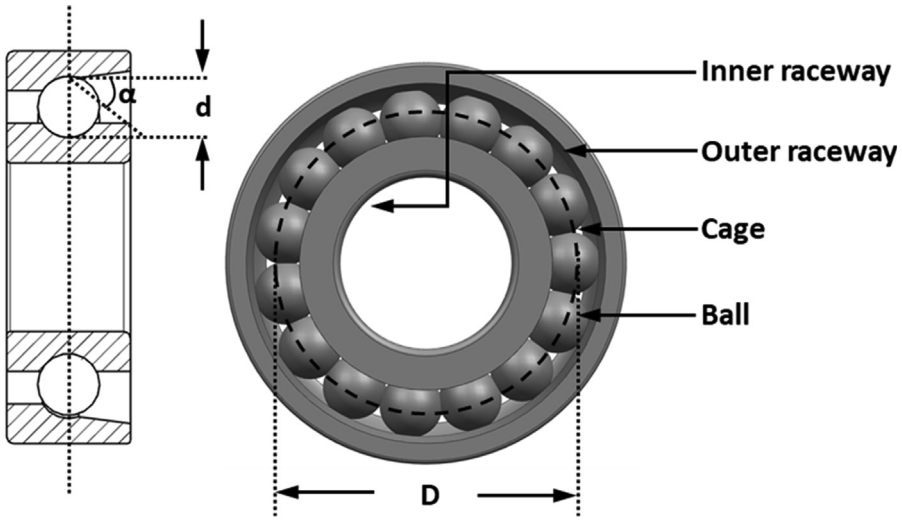

Fig. 2. Configuration of ball bearing used in the test.

Table 2
Test bearing specification.

Bearing type	Inner race diameter (mm)	Outer race diameter (mm)	Ball diameter (mm)	Number of rolling element	Dynamic load (N)
NSK 7202BW	15	35	6	11	7950

2.2. Acquired data

The RTF tests are conducted under the above-mentioned experimental conditions. Six data sets are obtained, all of which have visible faults after inspection. The raw acoustic signals are given in the upper figures of each data set in Fig. 12 (Section 4.2). The temporal behavior of the acoustic signals are different each other in terms of the initial period of constant magnitude, which range from less than 80 cycles in Fig. 12(d) to greater than 600 cycles in Fig. 12(f). The patterns of increase are also different, showing the abrupt increase in Fig. 12(a) and (c) or the gradual increase in Fig. 12(b) and (e). The spalls are present at the balls in all the data sets, while not all appear at the inner or outer races. As the representative examples, the spalls at the ball, inner and outer race are given in Fig. 3(a)~(c), respectively. In terms of spall size at the ball, Fig. 3(d)~(f) are also given to show the diverse size ranging from 200 μm to 5 mm. Overall speaking, the raw signals and resultant spalls are so diverse that it is indeed challenging to find out a universal HI useful for the prognosis.

2.3. Features of natural bearing faults

As mentioned earlier, many researchers have produced artificial faults for the fault detection and diagnosis study, as can be found in Lu et el. [29], Zhang et el. [8], and Yang et el. [30]. As shown in Fig. 3, however, the faults made over a number of cycles are different in nature, which have grown to a larger damage from several smaller faults, yielding irregular surface of pits and dents. Consequently, the characteristics of natural faults produced in this study are different from that of the artificial defects. As an example, Fig. 4 definitely shows the difference of natural and artificial fault signals acquired by the vibration sensor for 1 s with the 1200 rpm. Fig. 4(a) exhibits the clear periodicity of the signal with 20 Hz, which was induced by an artificial fault of size 1.0 mm at the inner race produced by the electric discharge machining (EDM). However, the natural fault signal with greater size 1.2 mm shows no such behavior due to the irregular shaped fault. This indicates that the artificial fault is of limited value in the prognostic study though easier to detect.

3. Description of the proposed approach

3.1. Overall process

In this section, process of fault prognosis based on the acoustic signal is addressed as given in the flowchart of Fig. 5, in which the frequency energy shift method (FESM) is employed to construct the health index (HI). It begins with the signal acquisition from the microphone sensor. Then the HI is extracted by the FESM, which is defined by the summation of the energies at those frequencies that show more pronounced increase than the others over the cycles (Section 3.2). At the initial

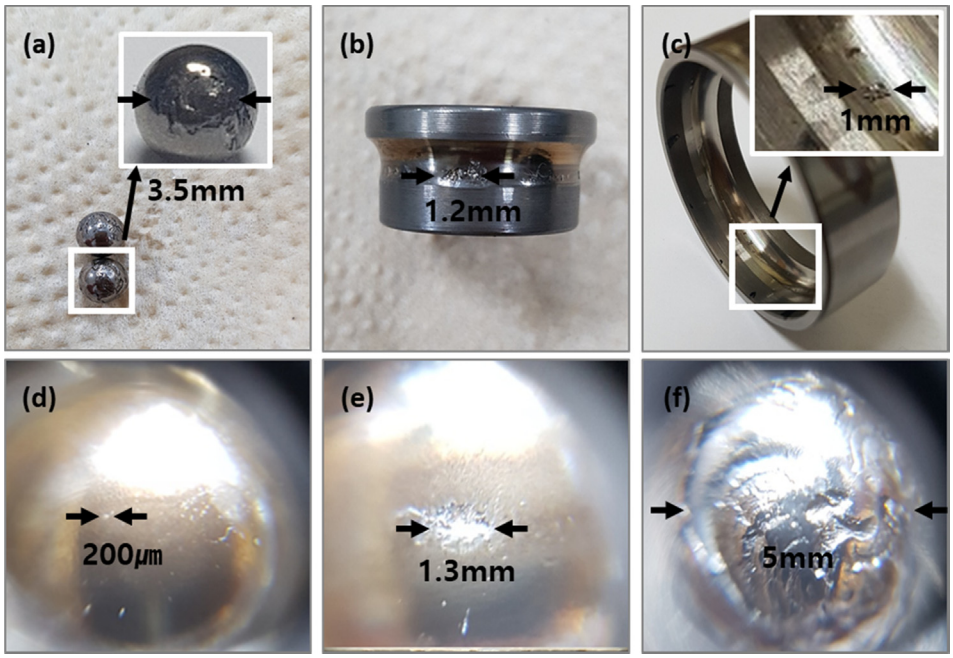

Fig. 3. Faults in the bearing components: (a) Ball (No.1), (b) Inner race (No.3), (c) Outer race (No.5), (d) Ball-small (No.6), (e) Ball-medium (No.3), (f) Ball-large (No.2). Note that the numbers in the parenthesis denote the data set ID.

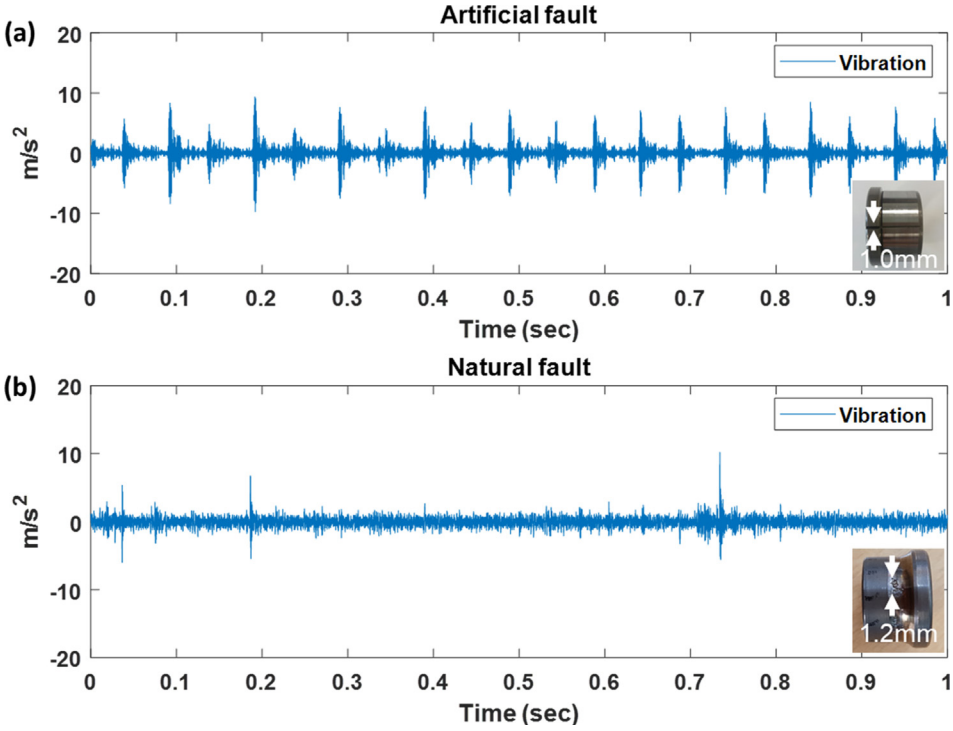

Fig. 4. Comparison of the fault signal: (a) artificial fault, (b) natural fault.

stage, the anomaly from the normal state is detected by monitoring the variance of HI over a window of recent cycles, and applying the Chi-square test (Section 3.3). Once detected, the HI begins to increase over time, which should be closely monitored for prognostic purpose. In order to assess the fault severity of HI relative to the failure level, failure threshold is defined based on the observations of the acoustic signal and its fault frequency amplitudes from the RTF data (Section 4.1). At last, the fault prognosis using the HI is implemented for the bearing (Section 4.2).

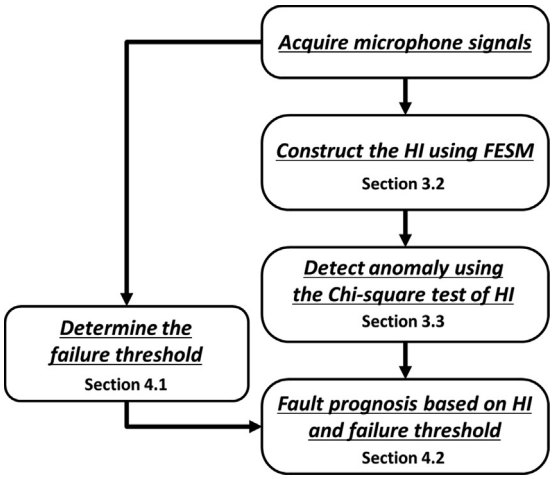

Fig. 5. A flowchart of fault prognosis using the HI made by FESM.

3.2. Frequency energy shifting method

According to the literature, the bearing fault development is divided into four stages as illustrated in Fig. 6 [31]. It shows the stages through the spectral analysis in the frequency domain. Ideally, normal bearing in Fig. 6(a) shows the only amplitude related with the frequency of the shaft rotation. As the fault commences, the bearing exhibits fault characteristics in the high frequency region as shown in the stage 1 in Fig. 6(b). However, at this stage, the bearing physically has no explicit faults. At stages 2 and 3, the signal corresponding to the natural frequency range of the bearing begins to appear, and the harmonics of the bearing fault frequency are gradually modulated by the shaft frequency. At the last stage in Fig. 6(e), the bearing fault grows to the visible size and the amplitude of the signal becomes even greater, in which a large number of modulation frequencies and its harmonics are generated. Overall speaking, the fault symptoms in the spectrum often starts at high frequency excitation and move to the lower frequencies as the damage progresses. The fault initiates with micro level at stage 1 and grows to the visible size at the last stage, which correspond in our study to the moment of anomaly detection and the moment that the failure threshold is reached.

In order to effectively assess the bearing health condition, it is important to select the proper features that can reflect the bearing fault status. The statistical features such as RMS, kurtosis, peak-to-peak or the envelope signal at fault frequencies are those common in the fault detection or diagnosis. However, these features are improper in terms of prognosis since they usually show low sensitivity to the fault progression or remain flat while rising only near the failure conditions. In this sense, it is important to extract better HI, which is capable of early detection, and shows gradual increase over the fault progression period.

In Fig. 6, we have observed that the bearing fault progression can be explained by the energy concentration or shift in specific frequency bands. Motivated by this, the HI is introduced here, in which the normalized energy is calculated to observe the temporal behavior of the energy concentration/shift.

$$E_i = {A_i}^2 / \sum_{k=1}^{F} {A_k}^2 \tag{1}$$

where A_i is the amplitude at ith frequency of the FFT at the current time, and E_i is its normalized energy. Spearman correlation is used to find E_i that shows strong correlation with the fault development, which is defined by

$$r_i = \frac{\mathrm{cov}\left(rg_t, rg_{E_i}\right)}{\sigma_{rg_t}\sigma_{rg_{E_i}}} \tag{2}$$

In this equation, rg_t and rg_{E_i} denote the ranks of the time t and energy E_i of ith frequency up to the current time, respectively. It represents the monotonicity between t and E_i. Better monotonicity indicates higher E_i as the time progresses. Once the normalized frequency energy E_i and its correlation coefficient r_i are calculated at the current time, sum of the top K energies with the largest correlation coefficients is calculated, and used as the HI as follows.

$$HI = \sum_{i \subset S} E_i \tag{3}$$

where the set S represents the top K frequencies with the largest correlation coefficients. In this study, K = 10 is employed.

3.3. Anomaly detection by Chi-square test of HI

During the initial period, the HI is used to detect anomaly by applying the Chi-square test to its variance over a time window, which is defined by

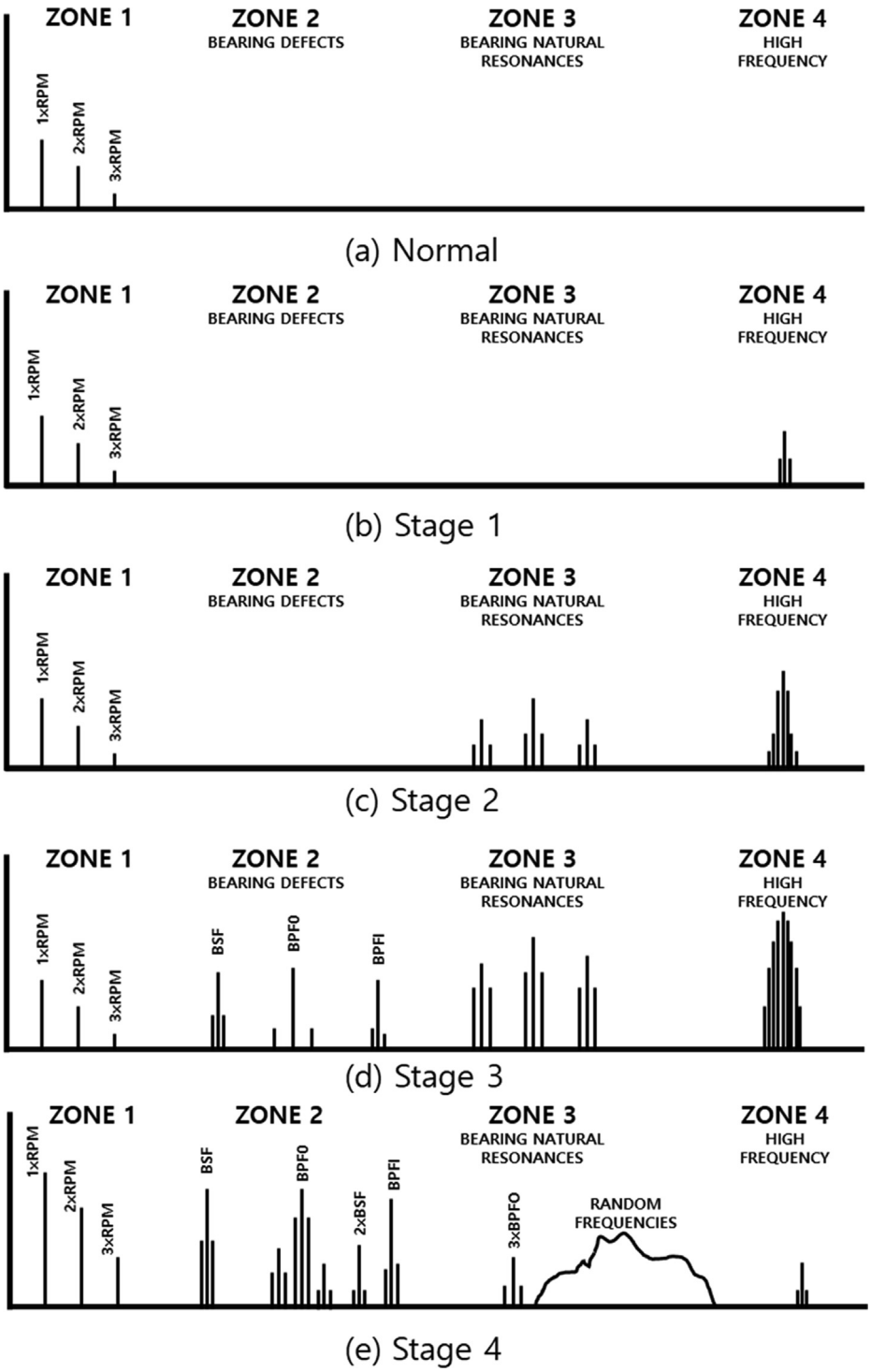

Fig. 6. The development stages of bearing faults [31].

$$\sigma_k{}^2 = \frac{1}{w-1}\sum_{i=k-w+1}^{k}(x_i - \bar{x})^2 \tag{4}$$

where x_i, $\bar{x}$, k, and w represent the HI value at ith cycle, its mean value for the time window over recent w cycles, current time index, and the time window size, respectively. Assuming the bearing as normal during the first-time window, which is denoted as σ_0^2, the test statistic is defined by

$$\chi_0{}^2 = \frac{(w-1)\sigma_k{}^2}{\sigma_0{}^2} \tag{5}$$

where χ_0^2 follows the Chi-square distribution with $w-1$ degree of freedom. If χ_0^2 exceeds the critical limit $\chi^2_{1-\alpha,w-1}$, it is considered anomaly with the confidence $(1-\alpha)$, which we call the moment of incipient fault detection. Once detected, it is expected that the HI starts increasing from this time. The process is illustrated in Fig. 7. In the implementation, the window size w is set as 15 and confidence as 90%.

In order to assess the current health level against failure, failure threshold should also be available based on some criteria, which often requires continued inspection of faults during the RTF experiment. Since this is not an easy task, in this study, the failure threshold is defined indirectly by examining the trend of raw acoustic signal as well as its spectrum amplitude at the fault characteristic frequencies. Note that the monitoring of fault frequencies are the most popular means of revealing and diagnosing the fault signatures in the bearing, which occurs by the impulsive response as the balls pass the spall area. They are the ball spin frequency (BSF), ball pass frequency of inner ring (BPFI), ball pass frequency of outer ring (BPFO) and fundamental train frequency (FTF), which are defined by the following equations [32].

$$BPFO = \frac{nf_r}{2}\left\{1 + \frac{\mathrm{d}}{\mathrm{D}}cos\alpha\right\} \tag{6}$$

$$BPFI = \frac{nf_r}{2}\left\{1 - \frac{\mathrm{d}}{\mathrm{D}}cos\alpha\right\} \tag{7}$$

$$FTF = \frac{f_r}{2}\left\{1 - \frac{\mathrm{d}}{\mathrm{D}}cos\alpha\right\} \tag{8}$$

$$BSF = \frac{Df_r}{d}\left\{1 - \left(\frac{\mathrm{d}}{\mathrm{D}}cos\alpha\right)^2\right\} \tag{9}$$

where D is the pitch diameter, d is the ball diameter,α is the contact angle between the ball and the cage, n is the number of rolling elements, and fr represents the rotating speed of bearing. Since the fault signals are usually modulated by resonant high frequency, envelope analysis is preceded before retrieving the frequencies [32,33] by the Hilbert transform. Once the threshold is established, current health level is assessed and monitored progressively over time between the values at the anomaly detection and the failure threshold.

4. Implementation of the proposed approach

4.1. Determination of failure threshold

As mentioned before, failure is defined in this study by monitoring the trend of the raw signal as well as its envelope spectra at the fault frequencies. If they show evident increase in common at some point in time, the failure is issued at the

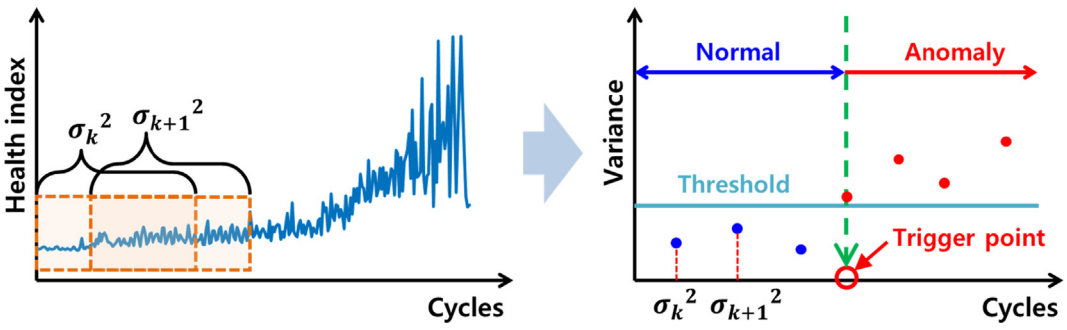

Fig. 7. Anomaly detection using Chi-square test of the variance of HI.

moment. Since both the vibration and acoustic signals are measured during the RTF tests, they are evaluated together for comparative purpose. Consider the data set No.3 as an example. Fig. 8(a) and (c) are the raw acoustic signal and its envelope magnitude at the fault frequencies of the acoustic signal. Fig. 8(b) and (d) are those for the vibration signal. In case of acoustic signal, the signals show evident increase from around 180 cycles, as marked by the red dotted line. In case of vibration signal, the tendency is similar but less clear: it is around 180 cycles for the raw signal, same as the acoustic case, whereas the BSF amplitude shows earlier increase at 160 cycles. Nevertheless, the signals state that it is the moment from which the faults develop in much greater fashion.

Consider next data set No.2 as another example. Fig. 9 shows the acoustic and vibration signals, given in the same way as Fig. 8. In this case, the acoustic signal shows clear increase from around 130 cycles as marked by red dotted line in both the

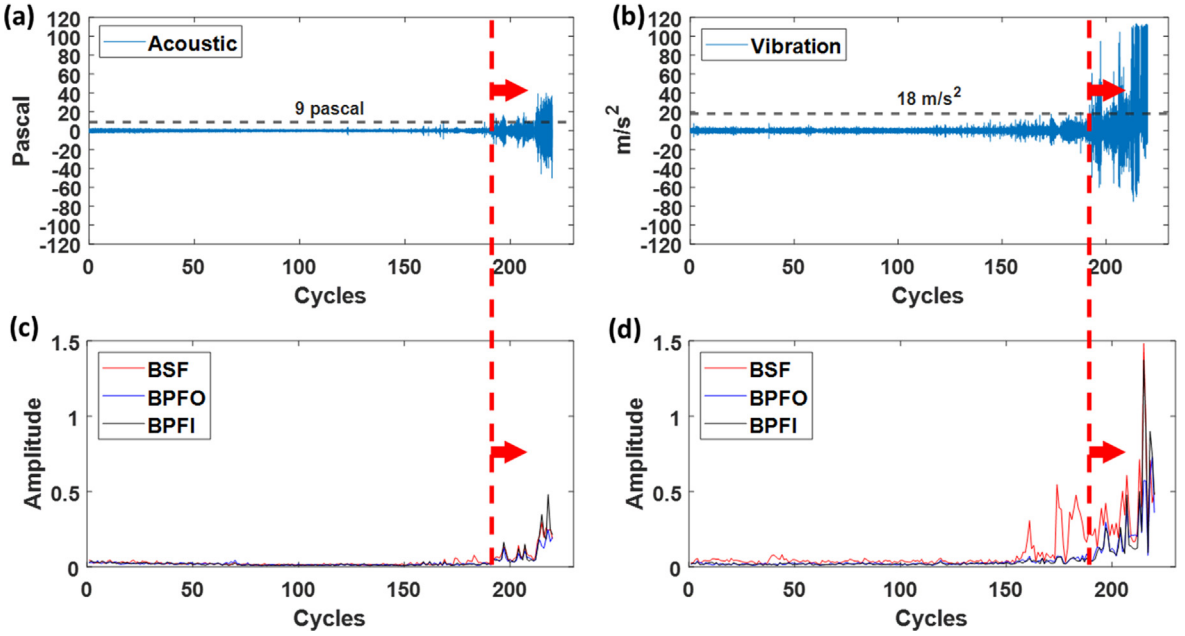

Fig. 8. Raw signals and fault frequency amplitudes of the acoustic data ((a) and (c)) and the vibration data ((b) and (d), for data set No.3.

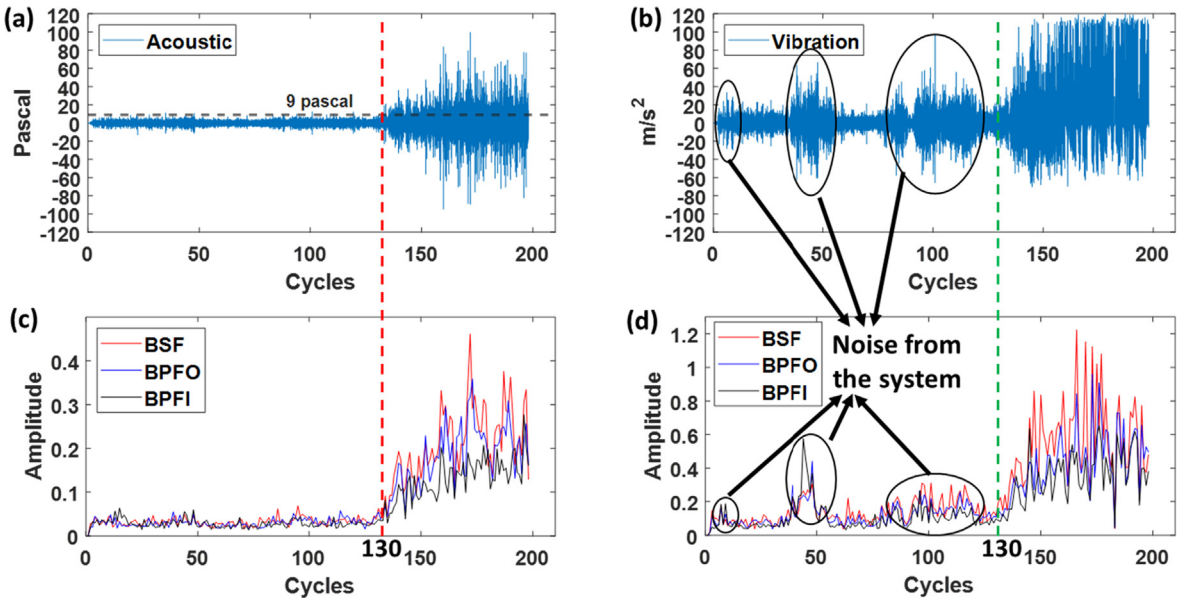

Fig. 9. Raw signals and fault frequency amplitudes of the acoustic data ((a) and (c)) and the vibration data ((b) and (d), for data set No.2.

raw signal and the fault frequencies, and there are no noticeable signal oscillations before 130 cycles. The vibration signal also shows increase from around 130 cycles as marked by the green dotted line. However, unlike the acoustic signal, it shows large oscillations at several moments before 130 cycles. The authors believe this as irrelevant to the bearing fault, which may have occurred by the noise from the system such as friction between the shaft and the support bearing. This may have been transmitted to the accelerometer attached to the bearing housing. The noise from the system has a significant effect on the behavior of bearing fault frequencies at the low frequency region mixed with the high frequency carrier signal. This phenomenon was also observed in the vibration signal of several other data sets. As a result, it is concluded that the signal acquired by the non-contact acoustic sensor is less influenced by the system noise than the contact vibration sensor.

By examining the acoustic signals of all the data sets, it is found that the acoustic signal and its envelope magnitude at the fault frequencies show increase in unison from certain cycles, which we define as the end of life (EOL) or failure time. In terms of the raw acoustic pressure, it takes place when the value exceeds 9 Pascal, which we define as the failure threshold. It is marked by the black dotted lines in Figs. 9 and 12 in the next section.

4.2. Health assessment via proposed health index

Frequency energy shifting method is applied to the data in order to monitor the health condition over time from the early stage. Fig. 10 shows the frequency energy change of the acoustic signal acquired during the RTF experiments for data set No.1. Fig. 10(a) and (b) indicate that the energy shifts occur over a band between 3×10^4 and 4×10^4 Hz, in which the energy increases approximately from around 200 cycles, which agrees with the trigger point of 224 cycles in Fig. 12(a). This is supposedly due to the creation and growth of the spalls at the micro level, which we call incipient fault.

In order to clarify the phenomenon of energy shift more effectively, Spearman correlation as given by equation (2) is monitored over the spectrum and time. Fig. 11 shows the result, in which the right bar denotes the coefficient value. In the figure, after 250 cycles, the correlation values increase at the three frequency bands with the red dotted box near the 3×10^4 Hz, 6×10^4 Hz and 7×10^4 Hz bands, respectively, which indicates that the frequency energy is shifted into the concentration at

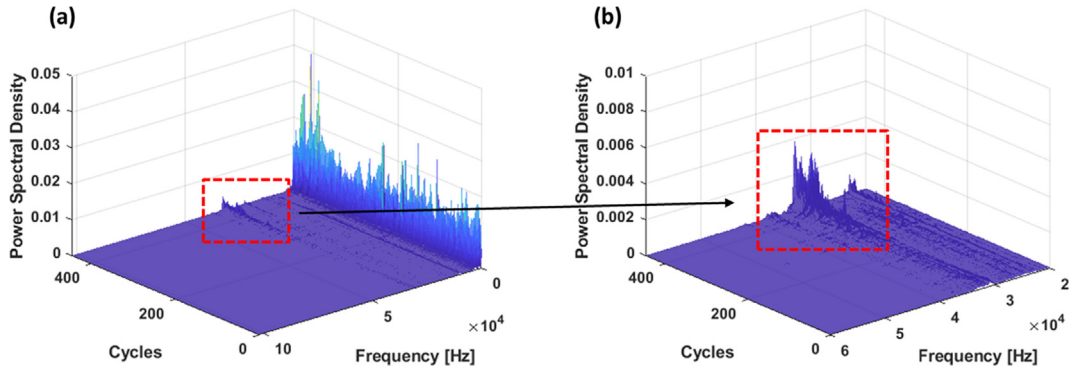

Fig. 10. (a) Frequency energy shift in the entire spectrum; (b) Enlarged view of frequency energy increase at the range of 3×10^4 and 4×10^4 Hz, for data set No.1.

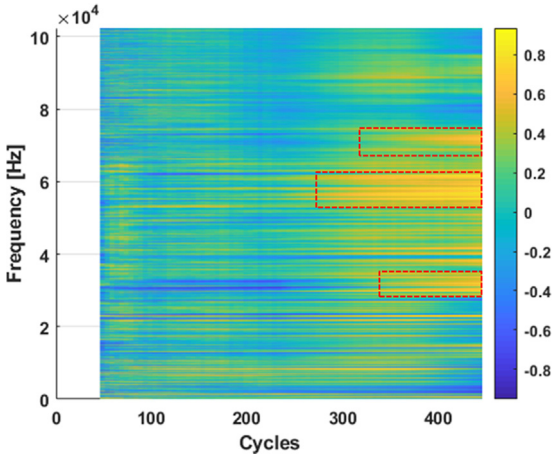

Fig. 11. Energy shift spectrogram using Spearman correlation depicted in the right bar, for data set No.2.

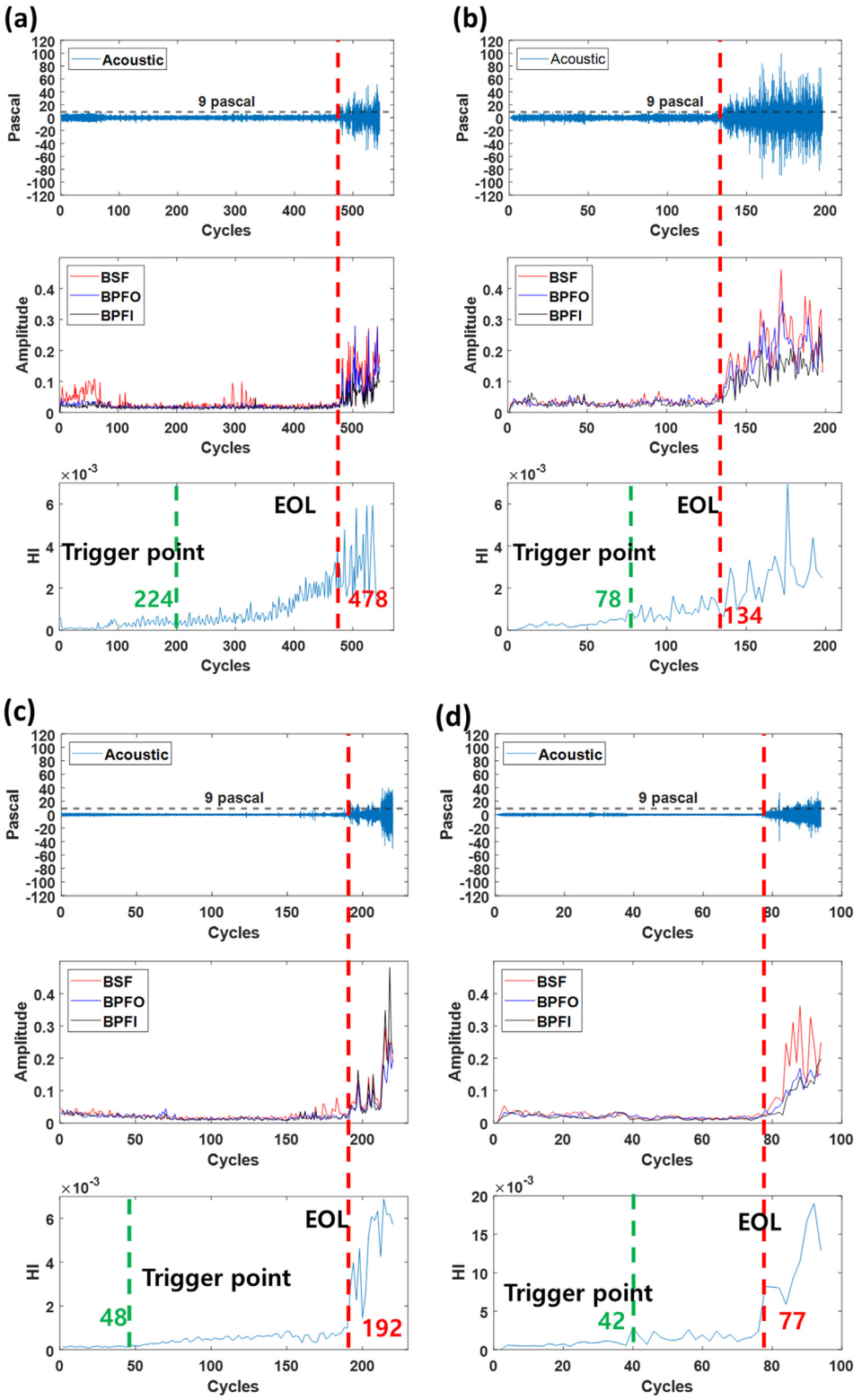

Fig. 12. Acoustic signal (top), fault frequency amplitudes (middle) and health index by FESM (bottom) over cycles for RTF data sets No.1 (a)~No.6 (f), respectively.

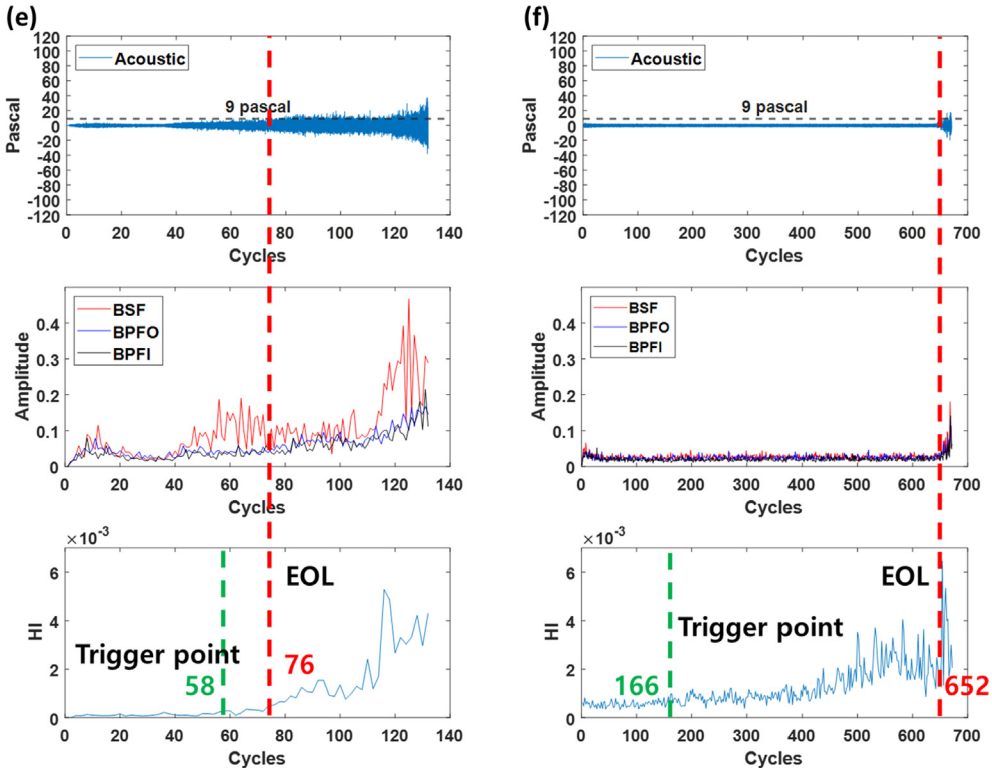

Fig. 12 (*continued*)

those bands with the largest at the middle. The HI defined in equation (3) is then calculated over time, which is the sum of 10 highest correlation coefficients of the energy spectrum over these frequency bands.

The HIs are given in the bottom figures for each data set in Fig. 12. In the figure, the trigger point and the EOL as defined in the previous section are given by the green and red dotted line, respectively. Note that the trigger point that indicates anomaly is much earlier than the EOL. The HI captures this and begins to increase afterwards, though they are gradual with more apparent (a, b, f) or lesser (c, d, e) degree. Although it is only one data set, Fig. 12(f) for the data set No.6 indicates that the test has been terminated right after the EOL, and faults are visually inspected. According to Fig. 3(d) of the set No.6, which is the picture showing the very small size of spall with 200 μm, it can be stated that the EOL is the onset of the visible fault. In other words, the HI represents the microscopic damage progression early before the moment that the fault grows to a visible spall size. It is made possible by the summation of the energies at those frequencies that show more pronounced increase than the others.

Note that the Fig. 12(e) for data set No.5 is different from the others, which does not show the distinct increase in both the raw signal and envelopes of fault frequencies, hence, is hard to find out the EOL clearly. This may have been caused by the BSF amplitude which has grown earlier than those of BPFO and BPFI. It indicates that the spall is introduced first at the ball, then induces the damage and propagates into the inner and outer race. Though much lesser degree, same phenomenon is also found at 180 cycles in Fig. 12(c), in which the BSF amplitude grows earlier before the EOL.

While the HI's in all the six data sets show increase over time, they also show substantial fluctuation. Usually these are filtered out using the signal processing technique such as the moving average, as is done in many literatures. The trend over time can then be modeled empirically via any functions, from which the current health level can be estimated and predicted for the remaining useful life (RUL). To do so, however, one needs to provide the corresponding failure threshold for the HI. In this study, the EOL's, i.e., the red dotted lines in Fig. 12 are applied to the HI's made by the RTF data, which is to extend the line down to the bottom figures. From the results, one can approximately set the threshold values of HI at somewhere between $1.5{\cdot}10^{-3}$~$2.0{\cdot}10^{-3}$ except the data set No.5, Fig. 12(e), which is less than $1.0{\cdot}10^{-3}$. Finding more exact threshold as well as predicting RUL is however another challenge, requiring much more experiments, hence is beyond the scope of this paper, being left as a future study.

5. Conclusions

A novel health index is proposed based on the microphone sensor to detect incipient fault of ball bearing and monitor its progression earlier than the visible fault appearance. Frequency energy shift method is employed to extract the health index

(HI), based on the findings that the energy is concentrated or shifted toward 2–3 specific frequency bands as the fault progresses. From the frequency bands, the top 10 frequencies extracted from the calculated Spearman correlations are used for HI. In the early stage, the anomaly or the onset of incipient fault is detected by the Chi-square test of the variance of HI made over a time window.

The end of life at which the visible faults appear is defined by the moment when the raw signal and its envelope spectrum at fault frequencies show distinct increase. Threshold is set by the raw acoustic pressure at 9 Pascal. It is found in all the data sets that the HI catches the incipient fault earlier than the visible fault presence, and show overall increase between the two moments, which may be of great advantage in view of predictive maintenance. Natural faults made by RTF experiments are used to demonstrate the approach. Comparing the microphone and vibration sensors, the performance of HI using the microphone sensor is superior to that of vibration sensor due to the advantage of non-contact sensing. It successfully performs early fault detection and monitors its progression against the threshold where the visible fault develops. Although not implemented in this paper, in light of how the HI is constructed, the authors believe that the HI may work well in the non-stationary operating conditions or the other types of bearing as long as the spall is considered as the fault in the prognosis study. Though the failure threshold is determined by the combined observations of raw signal and fault frequency amplitudes, it was by only one data set. Finding more exact threshold as well as predicting the RUL thereof is another challenge, requiring much more experiments. This may have to be left as a future study.

CRediT authorship contribution statement

Jaewoong Park: Investigation, Visualization, Validation, Writing - original draft. **Seokgoo Kim:** Validation, Software. **Joo-Ho Choi:** Conceptualization, Methodology, Supervision, Writing - review & editing. **Seung Hwan Lee:** Conceptualization, Methodology, Supervision, Writing - review & editing.

Declaration of Competing Interest

The authors declare that they have no known competing financial interests or personal relationships that could have appeared to influence the work reported in this paper.

Acknowledgement

This research was supported by a Korea Agency for Infrastructure technology Advancement (KAIA) in 2019 (19RTRPB104370-06-000000)

References

[1] D. Abboud, M. Elbadaoui, W. Smith, R. Randall, Advanced bearing diagnostics: a comparative study of two powerful approaches, Mech. Syst. Sig. Process. 114 (2019) 604–627.
[2] X. Zhang, Z. Liu, Q. Miao, L. Wang, Bearing fault diagnosis using a whale optimization algorithm-optimized orthogonal matching pursuit with a combined time–frequency atom dictionary, Mech. Syst. Sig. Process. 107 (2018) 29–42.
[3] S. Zhang, Q. He, K. Ouyang, W. Xiong, Multi-bearing weak defect detection for wayside acoustic diagnosis based on a time-varying spatial filtering rearrangement, Mech. Syst. Sig. Process. 100 (2018) 224–241.
[4] D. Barke, W. Chiu, Structural health monitoring in the railway industry: a review, Struct. Health Monitor. 4 (2005) 81–93.
[5] D. Macii, S. Dalpez, R. Passerone, M. Corrà, M. Avancini, L. Benciolini, A safety instrumented system for rolling stocks: methodology, design process and safety analysis, Measurement 67 (2015) 164–176.
[6] J. Lee, F. Wu, W. Zhao, M. Ghaffari, L. Liao, D. Siegel, Prognostics and health management design for rotary machinery systems—reviews, methodology and applications, Mech. Syst. Sig. Process. 42 (2014) 314–334.
[7] T. Momono, B. Noda, Sound and vibration in rolling bearings, Motion & Control 6 (1999) 29–37.
[8] D. Zhang, M. Entezami, E. Stewart, C. Roberts, D. Yu, Adaptive fault feature extraction from wayside acoustic signals from train bearings, J. Sound Vib. 425 (2018) 221–238.
[9] H. Akçay, S. Türkay, Power spectrum estimation in innovation models, Mech. Syst. Sig. Process. 121 (2019) 227–245.
[10] S. Mohanty, K.K. Gupta, K.S. Raju, Hurst based vibro-acoustic feature extraction of bearing using EMD and VMD, Measurement 117 (2018) 200–220.
[11] A. Glowacz, Fault diagnosis of single-phase induction motor based on acoustic signals, Mech. Syst. Sig. Process. 117 (2019) 65–80.
[12] B. Eftekharnejad, M. Carrasco, B. Charnley, D. Mba, The application of spectral kurtosis on acoustic emission and vibrations from a defective bearing, Mech. Syst. Sig. Process. 25 (2011) 266–284.
[13] C. Lim, S. Kim, Y.-H. Seo, J.-H. Choi, Feature extraction for bearing prognostics using weighted correlation of fault frequencies over cycles, Structural Health Monitoring, 0 1475921719900917.
[14] D. Siegel, C. Ly, J. Lee, Methodology and framework for predicting helicopter rolling element bearing failure, IEEE Trans. Reliab. 61 (2012) 846–857.
[15] E. Sutrisno, H. Oh, A.S.S. Vasan, M. Pecht, Estimation of remaining useful life of ball bearings using data driven methodologies, in: 2012 IEEE Conference on Prognostics and Health Management, IEEE, 2012, pp. 1–7.
[16] F. Camci, K. Medjaher, N. Zerhouni, P. Nectoux, Feature evaluation for effective bearing prognostics, Qual. Reliab. Eng. Int. 29 (2013) 477–486.
[17] B. Zhang, C. Sconyers, M. Orchard, R. Patrick, G. Vachtsevanos, Fault progression modeling: an application to bearing diagnosis and prognosis, in: Proceedings of the 2010 American Control Conference, IEEE, 2010, pp. 6993–6998.
[18] J. Wu, C. Wu, S. Cao, S.W. Or, C. Deng, X. Shao, Degradation data-driven time-to-failure prognostics approach for rolling element bearings in electrical machines, IEEE Trans. Ind. Electron. 66 (2018) 529–539.
[19] T.H. Loutas, D. Roulias, G. Georgoulas, Remaining useful life estimation in rolling bearings utilizing data-driven probabilistic e-support vectors regression, IEEE Trans. Reliab. 62 (2013) 821–832.
[20] D. An, J.-H. Choi, N.H. Kim, Remaining useful life prediction of rolling element bearings using degradation feature based on amplitude decrease at specific frequencies, Struct. Health Monitor. 17 (2018) 1095–1109.

[21] H. Qiu, J. Lee, J. Lin, G. Yu, Robust performance degradation assessment methods for enhanced rolling element bearing prognostics, Adv. Eng. Inf. 17 (2003) 127–140.
[22] L. Guo, N. Li, F. Jia, Y. Lei, J. Lin, A recurrent neural network based health indicator for remaining useful life prediction of bearings, Neurocomputing 240 (2017) 98–109.
[23] A. Rai, S. Upadhyay, An integrated approach to bearing prognostics based on EEMD-multi feature extraction, Gaussian mixture models and Jensen-Renyi divergence, Appl. Soft Comput. 71 (2018) 36–50.
[24] L. Duan, F. Zhao, J. Wang, N. Wang, J. Zhang, An integrated cumulative transformation and feature fusion approach for bearing degradation prognostics, Shock Vib. 2018 (2018) 9067184.
[25] X. Jin, Y. Sun, Z. Que, Y. Wang, T.W. Chow, Anomaly detection and fault prognosis for bearings, IEEE Trans. Instrum. Meas. 65 (2016) 2046–2054.
[26] P. Baraldi, G. Bonfanti, E. Zio, Differential evolution-based multi-objective optimization for the definition of a health indicator for fault diagnostics and prognostics, Mech. Syst. Sig. Process. 102 (2018) 382–400.
[27] J. Yu, A hybrid feature selection scheme and self-organizing map model for machine health assessment, Appl. Soft Comput. 11 (2011) 4041–4054.
[28] Y. Liu, X. Hu, W. Zhang, Remaining useful life prediction based on health index similarity, Reliab. Eng. Syst. Saf. 185 (2019) 502–510.
[29] S. Lu, P. Zheng, Y. Liu, Z. Cao, H. Yang, Q. Wang, Sound-aided vibration weak signal enhancement for bearing fault detection by using adaptive stochastic resonance, J. Sound Vib. 449 (2019) 18–29.
[30] B. Yang, Y. Lei, F. Jia, S. Xing, An intelligent fault diagnosis approach based on transfer learning from laboratory bearings to locomotive bearings, Mech. Syst. Sig. Process. 122 (2019) 692–706.
[31] S. F. A., Rolling Element Bearings, REB, Sales Technology, League City, Tex, USA, 2012.
[32] R.B. Randall, J. Antoni, Rolling element bearing diagnostics—a tutorial, Mech. Syst. Sig. Process. 25 (2011) 485–520.
[33] K. Shin, J. Hammond, Fundamentals of Signal Processing for Sound and Vibration Engineers, John Wiley & Sons, 2008.

Update

Mechanical Systems and Signal Processing

Volume 162, Issue , 1 January 2022, Page

DOI: https://doi.org/10.1016/j.ymssp.2021.108023

Mechanical Systems and Signal Processing 162 (2022) 108023

Contents lists available at ScienceDirect

Mechanical Systems and Signal Processing

journal homepage: www.elsevier.com/locate/ymssp

Corrigendum

Corrigendum to "Frequency energy shift method for bearing fault prognosis using microphone sensor" [Mech. Syst. Signal Process. 147 (2021) 107068]

Jaewoong Park [b,1], Seokgoo Kim [a,1], Joo-Ho Choi [a,*], Seung Hwan Lee [b,*]

[a] School of Aerospace and Mechanical Engineering, Korea Aerospace University, 76 Hanggongdae-gil, Deokyang-gu, Goyang-si, Gyeonggi-do 10540, Republic of Korea

[b] Department of Mechanical Convergence Engineering, Hanyang University, 222 Wangsimni-ro, Seongdong-gu, Seoul 04763, Republic of Korea

The authors regret the change of the affiliation.

<Jaewoong Park[1], Seokgoo Kim[1], Joo-Ho Choi*, Seung Hwan Lee*, School of Aerospace and Mechanical Engineering, Korea Aerospace University, 76 Hanggongdae-gil, Deokyang-gu, Goyang-si, Gyeonggi-do 10540, Republic of Korea>. The corrected author's affiliations are shown above.

The authors would like to apologise for any inconvenience caused.

DOI of original article: https://doi.org/10.1016/j.ymssp.2020.107068.

* Corresponding authors.

E-mail addresses: jhchoi@kau.ac.kr (J.-H. Choi), seunghlee@hanyang.ac.kr (S.H. Lee).

[1] Equally contributed as first authors, Graduate students.

https://doi.org/10.1016/j.ymssp.2021.108023

Available online 12 May 2021